System identification for FES-based tremor suppression

Engin H. Copur, Chris T. Freeman, Bing Chu, Dina S. Laila

www.elsevier.com/locate/ejcon

PII: S0947-3580(15)00131-4
DOI: http://dx.doi.org/10.1016/j.ejcon.2015.12.003
Reference: EJCON151

To appear in: *European Journal of Control*

Received date: 8 December 2014
Revised date: 8 September 2015
Accepted date: 1 December 2015

Cite this article as: Engin H. Copur, Chris T. Freeman, Bing Chu and Dina S Laila, System identification for FES-based tremor suppression, *Europea Journal of Control,* http://dx.doi.org/10.1016/j.ejcon.2015.12.003

SYSTEM IDENTIFICATION FOR FES-BASED TREMOR SUPPRESSION

Engin H. Copur[a,*], Chris T. Freeman[a], Bing Chu[a], Dina S. Laila[b]

[a] *Electronics and Computer Science, University of Southampton, Southampton, UK*
[b] *Engineering Sciences, University of Southampton, Southampton, UK*

Abstract

Tremor is an involuntary motion which is a common complication of Parkinson's disease and Multiple Sclerosis. A promising treatment is to artificially contract the muscle through application of induced electrical stimulation. However, existing controllers have either provided only modest levels of suppression or have been applied only in simulation. To enable more advanced, model-based control schemes, an accurate model of the relevant limb dynamics is required, together with identification procedures that are suitable for clinical application. This paper proposes such a solution, explicitly addressing limitations of existing methodologies. These include model structures that: (i) neglect critical features, and (ii) restrict the range of admissible control schemes, together with identification procedures that: (iii) employ stimulation inputs that are uncomfortable for patients, (iv) are overly complex and time-consuming for clinical use, and (v) cannot be automated. Experimental results confirm the efficacy of the proposed identification procedures, and show that high levels of accuracy can be achieved in a short identification time using test procedures that are suitable for future transference to the clinical domain.

Keywords: Tremor, System identification, Hammerstein structure, Functional electrical stimulation, Muscle model, Linearisation

1. Introduction

Tremor is a rhythmic, approximately periodic, oscillation that occurs in the limbs of patients with neurological disorders such as Multiple Sclerosis (MS) and Parkinson's disease. In 2008, 2.1 million people were diagnosed with MS worldwide [43] of which 25% to 58% suffered some form of tremor [26, 40]. In ballistic movements intention tremor is caused by delayed activation of the antagonist muscle to decelerate the initial agonist movement, causing overshoot, followed by delay in the activation of the second agonist to correct movement, thereby causing over-correction. It makes performing daily life activities very challenging, and may contribute to feelings of social isolation and depression. Invasive treatments are often considered too risky due to adverse effects after surgery and during long-term follow-up observations [18, 36, 38, 44]. Pharmacological methods have also not proved successful in treating intention tremor [11], hence there is increasing research interest in non-pharmacological treatment approaches.

Non-pharmacological treatment approaches such as tremor suppressing orthoses, limb cooling and limb weights are reviewed in [31] and have limitations. For example, limb cooling can reduce the amplitude and frequency of tremor but this effect is temporary, and is accompanied by a decrease in the nerve conduction velocity and muscle spindle activity. Moreover, deep cooling causes changes in muscle properties which mean that maximum voluntary forces will decrease [12]. Another technique comprises adding weights to tremulous limbs, however this causes fatigue and slowness in performing tasks. Examples of this type of tremor management system are tremor-suppressing orthoses [28, 35], which suppress tremor affecting the upper limb with either passive or active control. The main drawback of this system is that the presence of actuators and sensors on the affected limb is extremely inconvenient when performing daily life activities, causing fatigue, obstructing range of movement, and promoting feelings of self-consciousness due to their large size.

An alternative to active orthoses is Functional Electrical Stimulation (FES) which involves applying electrical impulses to artificially contract muscle. FES is typically applied using surface electrodes placed

*Corresponding author
Email addresses: ehc1g12@ecs.soton.ac.uk (Engin H. Copur), cf@ecs.soton.ac.uk (Chris T. Freeman), b.chu@ecs.soton.ac.uk (Bing Chu), D.Laila@soton.ac.uk (Dina S. Laila)

over relevant muscles using low cost hardware which is neither bulky nor obstructive to movement [25]. In [33, 34], FES was applied to suppress tremor at the wrist or elbow using filters implemented in a closed-loop feedback arrangement. This control structure was applied to three groups, comprising patients with (i) essential, (ii) Parkinsonian and (iii) cerebellar tremors associated with MS [34]. The results showed respective tremor reduction of 73%, 62% and 38%, respectively. Proportional plus derivative (PD) control was used in combination with fuzzy logic controller to suppress tremor in [45]. Simulation results showed that pathological tremor reduced by 85% but were not supported by experiments. An FES control strategy based on the modification of joint stiffness using a proportional plus integral (PI) action was proposed in [2], but with results showing only mild suppression of tremor. The aforementioned feedback approaches have well-known performance limitations, including a decrease in the robust stability margin as suppression increases over the required frequency range, together with an increase in undesirable low frequency distortion. These characteristics explain the limited ability of previous closed-loop FES controllers to suppress higher frequencies [2]. The difficulty in designing a stable feedback system with sufficient suppression is highlighted in [33], together with the tendency of the feedback system to produce large high-frequency stimulation transients which cause significant discomfort to patients.

To solve inherent limitations of feedback control for tremor suppression, one approach is a full characterization of both voluntary movement and tremor using electromyographic, electroencephalographic and kinematic signals [16]. However this necessitates employing a large amount of equipment which is a barrier to transference from the laboratory to the patient's local clinic or home.

To address these limitations more advanced controllers are required which exploit the known form of disturbance to embed feedforward predictive action. One example of this type is repetitive control (RC) that embeds a model of the disturbance within the control structure, with initial feasibility results presented in [42]. However such forms necessitate an accurate model of the underlying dynamics. The next section therefore reviews models that have been employed in FES control of tremor suppression, with focus on the wrist since this has received greatest research interest and is a critical component of upper limb tremor.

2. Dynamical Modelling of Wrist Joint in Tremor Suppression

A variety of biomechanical models exist that connect applied FES to resulting movement, with applications in rehabilitation, neuroprostheses and assistive technology fields [2, 13, 30, 32, 47]. Within tremor suppression, the model must also include a characterisation of both the tremulous motion and voluntary action in order to define the associated control problem [3, 17, 33, 45, 47].

In [33], a notch filter and a high-pass filter are employed in closed-loop FES controllers for the wrist and elbow joints. To identify the system model, FES was applied to the muscles of 6 unimpaired subjects at frequencies ranging from 1 to 12 Hz to produce extension and flexion. The amplitude and phase of the movement response were calculated for each subject. These were then averaged across subjects at each frequency and a linear transfer function was fitted to the resulting frequency response data. It is stated that the model is able to adequately predict gain margins, resonant frequencies and tremor attenuation. Unfortunately, the averaging process means the model poorly fits the response of individual subjects, especially at frequencies between 2 and 5 Hz. The fitting calculation also requires a large number of trial-and-error iterations. In addition, there are no model validation results. Closed-loop tests using the same model are reported in [34] and show some suppression of tremor when employed with MS patients. However there is no procedure to identify individual models for each patient, and instead the same linear model identified in [33] was employed, which accounts for the degraded performance.

Another strategy for tremor suppression at the wrist is based on co-contracting a pair of antagonist muscles to control the joint impedance with a simple PI controller equipped with anti-windup [3]. The wrist is approximated by a second order linear system including inertia, passive damping, passive stiffness, and gravity. The Hill-type muscle model is used to model the muscle contraction dynamics. An Extended Kalman Filter (EKF) is used to estimate the parameters of inertia, passive damping, passive stiffness and the maximum moment due to the gravity of the joint. Then a pseudorandom stimulation sequence is applied and the Gauss-Newton method is employed to identify the active parameters from the recorded joint motion. The accuracy of these methods is highly dependent on the initial values provided for each parameter set which are chosen arbitrarily. The procedure also involves FES signals that may be uncomfortable and give rise to involuntary muscle activation.

In [45, 47], a musculoskeletal model of the wrist involving an agonist/antagonist pair is simulated with a fuzzy logic control [45] or a neural oscillator [47] combined with a PD controller to suppress an external tremor signal. The wrist is modelled as a second order system with muscles taking the form of a Hill-type

model with the force-length (FL) property, the force-velocity (FV) property and the nonlinear muscle activation dynamics under isometric conditions. The parameters appearing in the model are taken from published literature and no procedure is presented to enable experimental identification.

The above studies highlight the absence of a model identification procedure that is suitable for clinical application. In this scenario controllers are required to perform satisfactorily, despite limited identification time available due to the onset of fatigue, changes in physiological conditions and subject availability constraints. Ideally, this procedure should also be able to be conducted by a clinician without the need for an engineer being present. Existing methods either: i) assume simplistic forms that inaccurately capture the dynamics (e.g. they negate a static dead zone and/or nonlinearity in torque generated), ii) utilise complex structures that give rise to procedures that can neither be applied in the time available, nor are aligned to subjects' needs, or iii) have not been validated in terms of the accuracy with which the model matches separate data sets. A suitable model must address these shortcomings by affecting a compromise between accuracy and ease of identification. This is further complicated since it is also desirable that the identification procedure yields a linear time-invariant (LTI) form to maximise the class of controllers subsequently employed.

Another key component of the model is that it should include a description of the tremor and voluntary motion dynamics. Tremor, especially intention tremor, has been found to occur at a frequency range between 3-5 Hz [11] and it has been shown that the wrist motions during daily life activities are usually generated at a frequency below 1 Hz [27]. The tremor frequency must be identified, and together with the frequency of voluntary action, can then be included in the controller design.

In the next section an approach is developed that combines a nonlinear model structure with an identification procedure that meets the demands of the clinical domain and is suitable for use with neurologically impaired subjects. The key contributions are as follows:

- To embed accuracy, the model structure incorporates nonlinear recruitment characteristics, together with a co-activation function created to minimize the effects of the dead-zone in the muscle torque.
- The structure can be linearised as a transparent manner to enable linear tremor suppression control design.
- The identification procedure is suitable for both patients and clinicians. Firstly, it is not time-consuming and can be carried out in less than 1 min. Secondly, it does not require user input and hence can be automated. Thirdly, it uses signals that are comfortable (have no sudden changes, such as present in random signals) and have been employed in previous clinical trials. Finally, it is able to explicitly identify the tremulous action (unlike [34]).
- Experimental results confirm the accuracy of the model both in fitting and prediction.

3. Problem Set-up

The proposed model comprises horizontal plane-flexion and extension wrist dynamics in response to FES applied to the Flexor Carpi Radialis (FCR) and Extensor Carpi Radialis (ECR) muscles, as well as an oscillatory movement due to tremor. Single joint motion can be accurately modelled through combination of rigid body dynamics (RBD) (characterising mass, inertia, damping and stiffness properties of limb segments) and a Hill-type model representing the response of muscle to the applied stimulation. Note that it is possible to include the neuromuscular reflex in the form of an additional dynamic function placed before the muscle model. However, it is neglected here since FES produces negligible effect on the reflex loop when applied transcutaneously, and hence on a macroscopic scale [39, 46].

In most applications, joint ranges and velocities are small so that the isometric behavior of muscle dominates [23] and additionally, muscle stretching and shortening have minor effect on the generated force because of the low amplitude and frequency of tremulous motion, and thus FL and FV components of the Hill-type model can be neglected. The activation dynamics component is almost uniformly represented by a Hammerstein structure. Recent works have shown that Hill-Huxley models [4, 5, 9] may be at least as accurate as a Hammerstein structure in representing the activation dynamics [15]. The drawback that their complexity undermines application to control has been countered by the proposal of a Hammerstein-Wiener structure [1], but as yet Hill-Huxley models have not been shown to extend to non-isometric conditions, and have not been used in controller derivation. In this paper a Hammerstein structure is therefore employed due to its popularity in the literature [22], confirmed accuracy, structural simplicity, and correspondence with biophysics. Within it, the Linear Activation Dynamics (LAD) models the muscle contraction dynamics and are preceded by a static mapping function, the Isometric Recruitment Curve

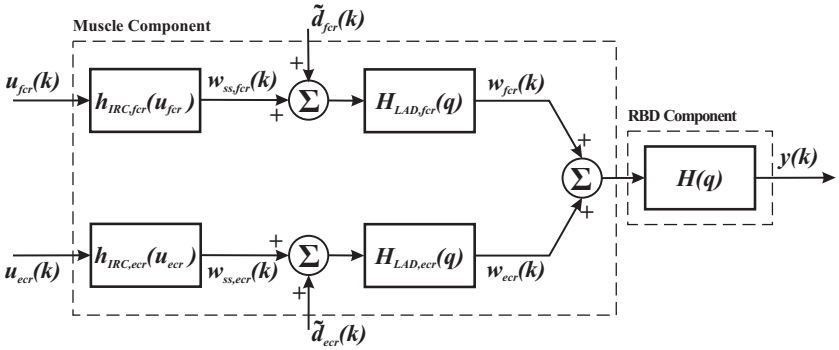

Fig. 1: General wrist model excited by FES and tremor signal

(IRC), which accounts for the static gain relation between the applied FES and the steady-state output torque when the muscle is held at a fixed length [10, 19].

In addition to the muscle dynamics, the joint dynamics of a human limb are commonly modelled by RBD in which the damping and elastic functions are linear [8, 20, 37]. This assumption has been used in previous research and is supported by experimental results over a wide range of movement.

3.1. Model Structure with the Application of Tremor

The above discussion motivates the overall model shown in Fig. 1, where $u_{fcr}(k)$ and $h_{IRC,fcr}(u)$ respectively denote the FES signal and the IRC of the FCR muscle, and similar notation is used for the ECR muscle. The terms $\tilde{d}_{fcr}(k)$ and $\tilde{d}_{ecr}(k)$ are general descriptions of tremor, each taking the form of a periodic moment acting on the relevant joint. The resulting muscle torque is then fed to the LAD which are represented by transfer functions $H_{LAD,fcr}(q)$ and $H_{LAD,ecr}(q)$ for the FCR and ECR, respectively. The corresponding two output torques, $w_{fcr}(k)$ and $w_{ecr}(k)$, are summed and applied to the RBD of the joint, which are also represented by a linear transfer function, $H(q)$. With this assumed model, the identification problem can now be defined as follows:

Devise a suitable set of input data $\{u_{fcr}(k), u_{ecr}(k)\}_{k=1,\ldots,N}$, together with an estimation procedure that yields a parameter vector estimate, $\hat{\theta}$, such that the norm of the difference between the measured and predicted outputs is minimised. Thus the minimization problem can be expressed as

$$\hat{\theta} := \arg\min_{\theta} \|\varepsilon\|_2 \tag{1}$$

with

$$\|\varepsilon\|_2 = \sqrt{\sum_{k=1}^{N} \left(y(k) - \hat{y}(k|k-1)\right)^2}. \tag{2}$$

Here $y(k)$ is the measured output and $\hat{y}(k|k-1)$ is the one-step-ahead predicted output associated with the assumed model description

$$\hat{y} = H(q,\theta)\Big\{H_{LAD,fcr}(q,\theta)\Big[\tilde{d}_{fcr}(\theta) + h_{IRC}(u_{fcr},\theta)\Big] + H_{LAD,ecr}(q,\theta)\Big[\tilde{d}_{ecr}(\theta) + h_{IRC}(u_{ecr},\theta)\Big]\Big\} + v \tag{3}$$

where v is a zero mean disturbance signal, and θ is the parameter vector. Note that the one-step-ahead predicted output $\hat{y}(k|k-1)$ satisfies

$$\min_{\hat{y}(k)} E(y(k) - \hat{y}(k)) \;\Rightarrow\; \hat{y}(k) = \hat{y}(k|k-1). \tag{4}$$

3.2. Model Assumptions and Co-activation

To simplify the model structure in Fig. 1 to enable computationally tractable solutions to the identification problem, the two-input one-output model is firstly transformed into a single-input single-output (SISO) model by combining the two input signals $u_{fcr}(k)$ and $u_{ecr}(k)$ into a single input signal $u(k)$. This is achieved with the mapping

$$u_{fcr} = \begin{cases} u + u_{coact,fcr} & u \geq 0 \\ u_{coact,fcr} & \text{otherwise} \end{cases} \tag{5}$$

$$u_{ecr} = \begin{cases} u_{coact,ecr} & u \geq 0 \\ u_{coact,ecr} - u & \text{otherwise} \end{cases} \tag{6}$$

where $u_{coact,fcr}$ and $u_{coact,ecr}$ are prescribed levels of co-activation for the FCR and ECR respectively. Using u and the summed relationship $w = w_{ss,fcr} + w_{ss,ecr}$, the two recruitment curves can be combined into a single static mapping between input u and steady-state torque w, given by

$$u \mapsto w, \qquad w = w_{ss,fcr} + w_{ss,ecr}$$
$$h_{IRC}(u) = \begin{cases} h_{IRC,fcr}(u + u_{coact,fcr}) - h_{IRC,ecr}(u_{coact,ecr}) & u \geq 0, \\ -h_{IRC,ecr}(-u + u_{coact,ecr}) + h_{IRC,fcr}(u_{coact,fcr}) & u \leq 0. \end{cases} \tag{7}$$

The co-activation levels must be chosen such that $h_{IRC,fcr}(u_{coact,fcr}) = h_{IRC,ecr}(u_{coact,ecr})$ in order for $u = 0$ to coincide with zero steady-state output torque. The co-activation has the effect of removing the dead zone inherent in each IRC, with an example shown in Fig. 2 where dashed and solid lines are used to denote $u_{coact} \neq 0$ and $u_{coact} = 0$, respectively.

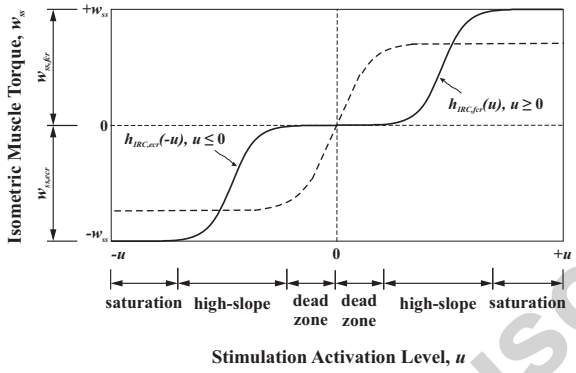

Fig. 2: IRC functions where solid and dashed lines represent h_{IRC} with and without co-activation, respectively.

Next, it is assumed that similar muscle groups have similar dynamics, so that $H_{LAD,fcr}(q) \approxeq H_{LAD,ecr}(q)$. This assumption is supported by the similar biophysical properties of the wrist flexors and extensors, and experimental evidence showing that their dynamic responses closely match [7]. Then both can be set equal to $H_{LAD}(q)$ which is further combined with $H(q)$ to form $P(q)$. In addition, since $\tilde{d}_{fcr}(k)$ and $\tilde{d}_{ecr}(k)$ are N_p-periodic and can be assumed to contain a maximum N_f harmonic, they can be written as

$$\tilde{d}_{fcr}(k) = A_0^{fcr} + \sum_{i=1}^{N_f} \left\{ A_i^{fcr} \cos\left(\frac{2\pi ik}{N_p}\right) + B_i^{fcr} \sin\left(\frac{2\pi ik}{N_p}\right) \right\}, \tag{8}$$

$$\tilde{d}_{ecr}(k) = A_0^{ecr} + \sum_{i=1}^{N_f} \left\{ A_i^{ecr} \cos\left(\frac{2\pi ik}{N_p}\right) + B_i^{ecr} \sin\left(\frac{2\pi ik}{N_p}\right) \right\} \tag{9}$$

and hence their sum is given by the N_p-periodic signal

$$\tilde{d}(k) = A_0 + \sum_{i=1}^{N_f} \left\{ A_i \cos\left(\frac{2\pi ik}{N_p}\right) + B_i \sin\left(\frac{2\pi ik}{N_p}\right) \right\} \tag{10}$$

with real values $A_i = A_i^{fcr} + A_i^{ecr}$ and $B_i = B_i^{fcr} + B_i^{ecr}$ for $i = 1, \ldots, N_f$. With these definitions, Fig. 1 is equivalent to Fig. 3a. Let the transfer function $P(q) \coloneqq B_P(q)/A_P(q)$. Since $B_P(q)$ is a finite impulse response (FIR) which is inherently stable and $\tilde{d}(k)$ is an N_p-periodic signal, $\lim_{i\to\infty} B_P(q)\tilde{d}(k + iN_P)$ has the form

$$A_0 A_0^P + \sum_{i=1}^{N_f} A_i A_i^P \cos\left(\frac{2\pi ik}{N_p}\right) + B_i B_i^P \sin\left(\frac{2\pi ik}{N_p}\right) \tag{11}$$

where A_i^P and B_i^P are real functions of $B_P(q)$. N_p-periodic signal $d(k)$ can then be placed as shown in Fig. 3b, which is identical to Fig. 3a given that the tremor signal is steady-state.

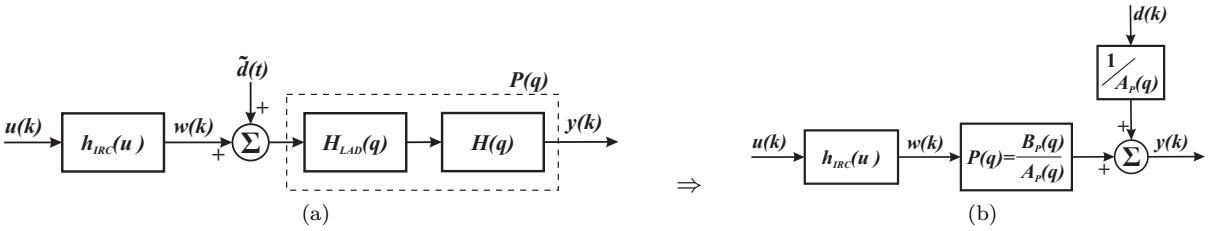

Fig. 3: Simplified wrist model: (a) Simplified model with co-activation, and (b) Simplified model with equivalent tremor signal representation

Remark. If only the fundamental frequency component is present in $\tilde{d}(k)$ and A_0 offset is present, then $N_f = 1$ giving

$$d(k) = A_0 A_0^P + A_1 A_1^P \cos\left(\frac{2\pi k}{N_p}\right) + B_1 B_1^P \sin\left(\frac{2\pi k}{N_p}\right).$$

3.3. System identification algorithm

In this subsection the components appearing in Fig. 3b are expressed explicitly as linear functions of their parameters. The form of external disturbance v is then stated, allowing the identification problem given by (1)-(4) to be solved.

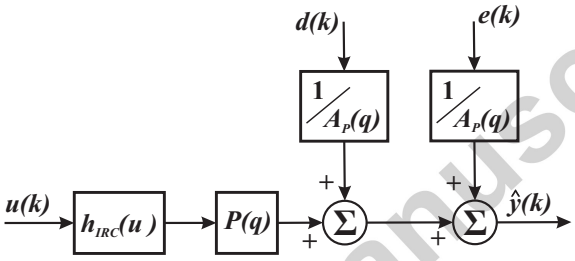

Fig. 4: ARX type model structure of the wrist model

3.3.1. Mathematical representation of system identification problem

The linear dynamics of the wrist model take the polynomial form

$$P(q) = \frac{B_P(q)}{A_P(q)} = \frac{b_0 q^{-m_P} + b_1 q^{-(m_P+1)} + \ldots + b_{n_P} q^{-(m_P+n_P)}}{1 + a_1 q^{-1} + \ldots + a_{l_P} q^{-l_P}} \tag{12}$$

where n_p, l_p and m_p denote the number of zeros, poles and the time delay order, respectively. Te coefficients of polynomial can be written in a vector form

$$\theta_{l_P} = \begin{bmatrix} \theta_{a_P} \\ \theta_{b_P} \end{bmatrix} = [a_1 \ \ldots \ a_{l_P} \ b_0 \ b_1 \ \ldots \ b_{n_P}]^T.$$

Since $h_{IRC,fcr}(u)$ and $h_{IRC,ecr}(u)$ can be represented as polynomial functions [22], the continuous compound function $h_{IRC}(u)$ can be represented by the form

$$h_{IRC}(u) = \beta_0 + \beta_1 u + \ldots + \beta_{m-1} u^{m-1} + \beta_m u^m. \tag{13}$$

This gives rise to nonlinear parameter vector $\theta_n = [\beta_0 \ \beta_1 \ \ldots \ \beta_m]^T$. Lastly, since $d(k)$ comprises N_f frequency, (11) can be written in the matrix form:

$$d(k) = \underbrace{\left[1 \ \cos\left(\frac{2\pi k}{N_p}\right) \ \sin\left(\frac{2\pi k}{N_p}\right) \ \cdots \ \cos\left(\frac{2\pi N_f k}{N_p}\right) \ \sin\left(\frac{2\pi N_f k}{N_p}\right)\right]}_{X} \underbrace{\left[\lambda_0 \ \lambda_1^A \ \lambda_1^B \ \cdots \ \lambda_{N_f}^A \ \lambda_{N_f}^B\right]^T}_{\theta_d} := d(\theta_d) \tag{14}$$

where $\lambda_0, \lambda_1^A, \lambda_1^B, \ldots, \lambda_{N_f}^A, \lambda_{N_f}^B$ are scalar amplitudes. This yields parameter vector $\theta_d = [\lambda_0 \lambda_1^A \lambda_1^B \cdots \lambda_{N_f}^A \lambda_{N_f}^B]^T$.

The parameters corresponding to linear model components can be grouped into the linear parameter vector $\theta_l = \left[\theta_{l_p} \ \theta_d\right]^T$, so that the composite parameter vector is given by $\theta = [\theta_n \ \theta_l]^T$. It is now necessary to provide a precise form of the external disturbance signal, v, appearing in (3). This is

selected as $v(k) = A_P(q)^{-1}e(k)$, where e is zero mean white noise, leading to the overall autoregressive exogenous (ARX) model structure shown in Fig. 4.

Substituting the foregoing expressions into (3) the model description can be written as

$$\hat{y}(k) = \frac{B_P(q)}{A_P(q)} h_{IRC}(u(k), \hat{\theta}_n) + \frac{1}{A_P(q)} d(k) + \frac{1}{A_P(q)} e(k). \tag{15}$$

Using (15) and following [24], the corresponding one-step-ahead minimising solution to (4) is then given by

$$\hat{y}(k|k-1) = B_P(q) h_{IRC}(u(k), \hat{\theta}_n) + [1 - A_P(q)]y(k) + d(k).$$

Hence the prediction error $\varepsilon(k)$ appearing in (2) is

$$\varepsilon(k) = y(k) - \hat{y}(k|k-1) = A_P(q)y(k) - B_P(q)h_{IRC}(u(k), \hat{\theta}_n) - d(k). \tag{16}$$

Next note that the biophysical properties of muscle mean that the function (13) is monotonically increasing. Thus θ_n should be estimated such that $h_{IRC}(u)$ is a strictly increasing continuous function on $[u_{min}, u_{max}]$ with $h_{IRC}(u)$ differentiable at each point $u_0 \in (u_{min}, u_{max})$. This corresponds to the condition

$$\left.\frac{dh_{IRC}}{du}\right|_{u=u_0} = \beta_1 + \ldots + \beta_{m-1}(m-1)u^{m-2} + \beta_m m u^{m-1} \geq 0. \tag{17}$$

Substituting (16) into (1), the identification problem (1) now becomes

$$\hat{\theta} = \arg\min_{\theta} \left\| A_P(q)y - B_P(q)h_{IRC}(u, \hat{\theta}_n) - d(\hat{\theta}_d) \right\|_2 \tag{18}$$

subject to the constraint of (17).

3.3.2. Nonlinear parameter identification

The problem (18) cannot be solved using standard methods due to its nonlinearity, and hence, an iterative scheme is now proposed. This involves firstly identifying nonlinear parameter θ_n using fixed θ_l, and subsequently identifying linear parameter θ_l with fixed θ_n. The former optimisation is given by

$$\hat{\theta}_n = \arg\min_{\theta_n} \left\| A_P(q)y - B_P(q)\, h_{IRC}(u, \hat{\theta}_n) - d(\hat{\theta}_d) \right\|_2 \qquad \text{subject to} \qquad A\theta_n \geq 0 \tag{19}$$

where the constraint enforces monotonic condition (17). From (13), it follows that $h_{IRC}(u, \theta_n)$ is linear in θ_n, and hence

$$\begin{aligned}(\hat{B}_P(q)\, h_{IRC}(u, \hat{\theta}_n))(k) =& \beta_0 \underbrace{\left(\hat{b}_0 + \cdots + \hat{b}_{n_P}\right)}_{h_{IRC_0}(u(k), \hat{\theta}_{b_P})} + \beta_1 \underbrace{\left(\hat{b}_0 u(k-m_P) + \cdots + \hat{b}_{n_P} u(k-m_P-n_P)\right)}_{h_{IRC_1}(u(k), \hat{\theta}_{b_P})} \\ &+ \cdots + \beta_m \underbrace{\left(\hat{b}_0 u(k-m_P)^m + \cdots + \hat{b}_{n_P} u(k-m_P-n_P)^m\right)}_{h_{IRC_m}(u(k), \hat{\theta}_{b_P})}.\end{aligned} \tag{20}$$

(19) can be rewritten as the constrained linear least-squares problem

$$\hat{\theta}_n = \arg\min_{\theta_n} \left\| Y_n\left(y, \hat{\theta}_{a_P}\right) - \Phi_n\left(u, \hat{\theta}_{b_P}\right)\hat{\theta}_n - D(\hat{\theta}_d) \right\|_2 \qquad \text{subject to} \qquad A\theta_n \geq 0 \tag{21}$$

where

$$A = \begin{bmatrix} 0 & 1 & \cdots & (m-1)u(l_P+1)^{m-2} & mu(l_P+1)^{m-1} \\ 0 & 1 & \cdots & (m-1)u(l_P+2)^{m-2} & mu(l_P+2)^{m-1} \\ \vdots & \vdots & & \vdots & \vdots \\ 0 & 1 & \cdots & (m-1)u(N)^{m-2} & mu(N)^{m-1} \end{bmatrix},$$

$$Y_n\left(y, \hat{\theta}_{a_P}\right) = \begin{bmatrix} y(l_P+1) + \hat{a}_1 y(l_P) + \cdots + \hat{a}_{l_P} y(1) \\ y(l_P+2) + \hat{a}_1 y(l_P+1) + \cdots + \hat{a}_{l_P} y(2) \\ \vdots \\ y(N) + \hat{a}_1 y(N-1) + \cdots + \hat{a}_{l_P} y(N-l_P) \end{bmatrix},$$

$$\Phi_n\left(u,\hat{\theta}_{b_P}\right)=\begin{bmatrix} h_{IRC_0}(u(l_P+1),\hat{\theta}_{b_P}) & \cdots & h_{IRC_m}(u(l_P+1),\hat{\theta}_{b_P}) \\ h_{IRC_0}(u(l_P+2),\hat{\theta}_{b_P}) & \cdots & h_{IRC_m}(u(l_P+2),\hat{\theta}_{b_P}) \\ \vdots & & \vdots \\ h_{IRC_0}(u(N),\hat{\theta}_{b_P}) & \cdots & h_{IRC_m}(u(N),\hat{\theta}_{b_P}) \end{bmatrix}$$

and

$$D(\hat{\theta}_d)=\begin{bmatrix} \hat{\lambda}_0+\hat{\lambda}_1^A\cos\frac{2\pi(l_P+1)}{N_p}+\hat{\lambda}_1^B\sin\frac{2\pi(l_P+1)}{N_p}+\cdots+\hat{\lambda}_{N_f}^A\cos\frac{2\pi N_f(l_P+1)}{N_p}+\hat{\lambda}_{N_f}^B\sin\frac{2\pi N_f(l_P+1)}{N_p} \\ \hat{\lambda}_0+\hat{\lambda}_1^A\cos\frac{2\pi(l_P+2)}{N_p}+\hat{\lambda}_1^B\sin\frac{2\pi(l_P+2)}{N_p}+\cdots+\hat{\lambda}_{N_f}^A\cos\frac{2\pi N_f(l_P+2)}{N_p}+\hat{\lambda}_{N_f}^B\sin\frac{2\pi N_f(l_P+2)}{N_p} \\ \vdots \\ \hat{\lambda}_0+\hat{\lambda}_1^A\cos\frac{2\pi N}{N_p}+\hat{\lambda}_1^B\sin\frac{2\pi N}{N_p}+\cdots+\hat{\lambda}_{N_f}^A\cos\frac{2\pi N_f N}{N_p}+\hat{\lambda}_{N_f}^B\sin\frac{2\pi N_f N}{N_p} \end{bmatrix}$$

$$=\underbrace{\begin{bmatrix} 1 & 1 & \cdots & 1 & 1 \\ \cos\frac{2\pi(l_P+1)}{N_p} & \sin\frac{2\pi(l_P+1)}{N_p} & \cdots & \cos\frac{2\pi N_f(l_P+1)}{N_p} & \sin\frac{2\pi N_f(l_P+1)}{N_p} \\ \cos\frac{2\pi(l_P+2)}{N_p} & \sin\frac{2\pi(l_P+2)}{N_p} & \cdots & \cos\frac{2\pi N_f(l_P+2)}{N_p} & \sin\frac{2\pi N_f(l_P+2)}{N_p} \\ \vdots & \vdots & & \vdots & \vdots \\ \cos\frac{2\pi N}{N_p} & \sin\frac{2\pi N}{N_p} & \cdots & \cos\frac{2\pi N_f N}{N_p} & \sin\frac{2\pi N_f N}{N_p} \end{bmatrix}}_{X}\underbrace{\begin{bmatrix} \hat{\lambda}_0 \\ \hat{\lambda}_1^A \\ \hat{\lambda}_1^B \\ \vdots \\ \hat{\lambda}_{N_f}^A \\ \hat{\lambda}_{N_f}^B \end{bmatrix}}_{\hat{\theta}_d}.$$

This type of linear least squares problem can be readily solved, e.g. using MATLAB function, *fmincon*.

3.3.3. Linear parameter identification

Given an estimate $\hat{\theta}_n$ of nonlinear parameter vector θ_n, cost function (18) can be minimized with respect to the linear parameter vector. This linear least squares minimization problem is given by

$$\hat{\theta}_l=\arg\min_{\theta_l}\left\|A_P(q)y-B_P(q)\,h_{IRC}(u,\hat{\theta}_n)-d(\hat{\theta}_d)\right\|_2$$

where

$$B_P(q)\,h_{IRC}(u,\hat{\theta}_n)=b_0\underbrace{\left[\hat{\beta}_m u(k-m_P)^m+\hat{\beta}_{m-1}u(k-m_P)^{m-1}+\ldots+\hat{\beta}_1 u(k-m_P)+\hat{\beta}_0\right]}_{h_{IRC}\left(u(k-m_P),\hat{\theta}_n\right)}+\cdots$$
$$+\,b_{n_P}\underbrace{\left[\hat{\beta}_m u(k-m_P-n_P)^m+\hat{\beta}_{m-1}u(k-m_P-n_P)^{m-1}+\ldots+\hat{\beta}_1 u\,(k-m_P-n_P)+\hat{\beta}_0\right]}_{h_{IRC}\left(u(k-m_P-n_P),\hat{\theta}_n\right)},$$

or equivalently in matrix form

$$\hat{\theta}_l=\arg\min_{\theta_l}\left\|Y_l-\Phi_l\left(u,y,\hat{\theta}_n\right)\theta_{l_P}-X\hat{\theta}_d\right\|_2 \tag{22}$$

where

$$Y_l=\left[y\,(l_P+1)\;\;y\,(l_P+2)\;\;\ldots\;\;y\,(N)\right]^T,$$

$$\Phi_l\left(u,y,\hat{\theta}_n\right)=\begin{bmatrix} -y\,(l_P) & \cdots & -y\,(1) & h_{IRC}(u(l_P+1-m_P),\hat{\theta}_n) & \cdots & h_{IRC}(u(l_P+1-m_P-n_P),\hat{\theta}_n) \\ -y\,(l_P+1) & \cdots & -y\,(2) & h_{IRC}(u(l_P+2-m_P),\hat{\theta}_n) & \cdots & h_{IRC}(u(l_P+2-m_P-n_P),\hat{\theta}_n) \\ \vdots & & \vdots & \vdots & & \vdots \\ -y\,(N-1) & \cdots & -y\,(N-l_P) & h_{IRC}(u(N-m_P),\hat{\theta}_n) & \cdots & h_{IRC}(u(N-m_P-n_P),\hat{\theta}_n) \end{bmatrix} \tag{23}$$

and

$$X=\begin{bmatrix} 1 & 1 & \cdots & 1 & 1 \\ \cos\frac{2\pi(l_P+1)}{N_p} & \sin\frac{2\pi(l_P+1)}{N_p} & \cdots & \cos\frac{2\pi N_f(l_P+1)}{N_p} & \sin\frac{2\pi N_f(l_P+1)}{N_p} \\ \cos\frac{2\pi(l_P+2)}{N_p} & \sin\frac{2\pi(l_P+2)}{N_p} & \cdots & \cos\frac{2\pi N_f(l_P+2)}{N_p} & \sin\frac{2\pi N_f(l_P+2)}{N_p} \\ \vdots & \vdots & & \vdots & \vdots \\ \cos\frac{2\pi N}{N_p} & \sin\frac{2\pi N}{N_p} & \cdots & \cos\frac{2\pi N_f N}{N_p} & \sin\frac{2\pi N_f N}{N_p} \end{bmatrix}. \tag{24}$$

Concatenating (23) and (24) horizontally yields

$$\Phi_{ld}\left(u, y, \hat{\theta}_n, X\right) = \left[\begin{array}{cc} \Phi_l\left(u, y, \hat{\theta}_n\right) & X \end{array}\right].$$

Hence (22) can be rewritten in the form of

$$\hat{\theta}_l = \arg\min_{\theta_l} \left\| Y_l - \Phi_{ld}\left(u, y, \hat{\theta}_n, X\right)\theta_l \right\|_2. \tag{25}$$

The solution of (25) is

$$\hat{\theta}_l = \left(\Phi_{ld}\left(u, y, \hat{\theta}_n, X\right)^T \Phi_{ld}\left(u, y, \hat{\theta}_n, X\right)\right)^{-1} \Phi_{ld}\left(u, y, \hat{\theta}_n, X\right)^T Y_l.$$

3.3.4. Algorithmic summary

Minimization over the θ_n and θ_{ld} parameters can be executed iteratively assuming the initial linear component values $\hat{\theta}_l^0$ and $\hat{\theta}_d^0$, an input/output data set $\{u(k),\, y(k)\}_{k=1,2,\ldots,N}$ and a convergence tolerance ϵ. This yields Algorithm 1:

Algorithm 1: Iterative algorithm for identifying the parameter vector θ

$\mathtt{j} = 0;$

repeat

  $\mathtt{j} = \mathtt{j} + 1;$

  $\hat{\theta}_n^j = \arg\min_{\theta_n} \left\| A_P(q)y - B_P(q)h_{IRC}(u, \hat{\theta}_n^j) - d(\hat{\theta}_d^j) \right\|_2$ subject to (17);

  $\hat{\theta}_l^j = \left(\Phi_{ld}\left(u, y, \hat{\theta}_n^j, X\right)^T \Phi_{ld}\left(u, y, \hat{\theta}_n^j, X\right)\right)^{-1} \Phi_{ld}\left(u, y, \hat{\theta}_n^j, X\right)^T Y_l;$

until $\left| V_N\left(\hat{\theta}_l^j, \hat{\theta}_n^j\right) - V_N\left(\hat{\theta}_l^{j-1}, \hat{\theta}_n^{j-1}\right) \right| < \epsilon;$

Output: $\hat{\theta} = \left[\hat{\theta}_n^j\ \hat{\theta}_l^j\right]^T$

4. Experimental Evaluation

4.1. Experimental Set-up

In order to evaluate the identification procedure developed in Section 3, tests have been conducted using a validated instrumented wrist rig which has previously been used in clinical trials to assess impairment in stroke. This is described in [41] and is shown in Fig. 5. To measure the angular position y at the wrist joint, the wrist rig is fitted with a potentiometer which is calibrated before use. The rig supports the forearm using an inflatable cuff in a molded splint to prevent any movement at the elbow and shoulder joints. Using standard guidelines [14], two sets of PALS Plus surface electrodes are placed on the forearm to stimulate the FCR and ECR muscles.

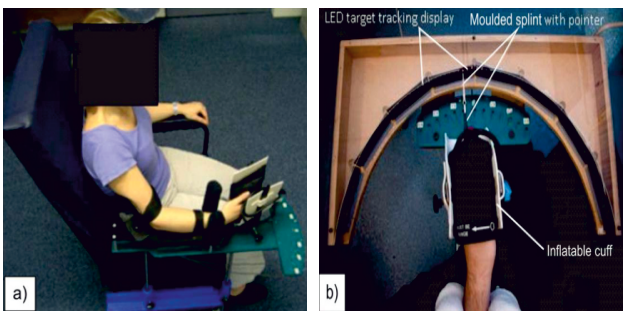

Fig. 5: Experimental set-up (Permission obtained to reproduce [41]) showing a) how the participant's arm is supported by the wrist rig b) an overhead view of the wrist.

In this study testing was conducted with four male unimpaired participants using their right arm. For each participant, data collection comprised two experiments separated by a rest period of 20 minutes

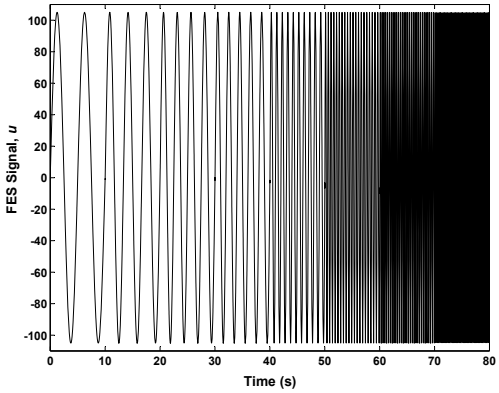

Fig. 6: Input signal used for the estimation of relationship between wrist joint angle and torque

in order to prevent muscle fatigue. Each experiment consisted of a prediction trial and a validation trial, each lasting for approximately 3 minutes, which together are termed a "data set". Another rest period was taken for at least 10 minutes between each trial in order to reduce effects of muscle fatigue. Additionally, the electrode pads were not moved between experiments and no change was made in FES amplitude settings.

The aim of the trial is not only to evaluate the accuracy of the model but also to establish whether parameters m_P, n_P and l_P can be fixed in advance. This is necessary to enable efficient clinical application. The input/output set associated with each trial can be written as follows:

$$Z_i^N = \{u_i(1), y_i(1), u_i(2), y_i(2), \ldots, u_i(N), y_i(N)\} \tag{26}$$

where i denotes the trial number, of which a total of 4 were performed for each participant. For each set of data obtained from the experiment, Algorithm 1 was applied. In order to provide sufficient excitation, the input u was chosen to comprise a set of sinewaves that spanned the frequency range from 0.2 to 4 Hz as shown in Fig. 6. This captures a substantial component of the range of voluntary motion (0-1 Hz) [27], and the typical tremor range (2.5-5 Hz) [29]. Higher frequencies were not used due to their inherent attenuation by the arm dynamics. Eight frequencies over this range were applied separately, since the form of the signal has been found to be well-tolerated by patients. Note that this signal form has been shown to be sufficiently exciting over the system bandwidth, while white band-limited noise causes discomfort or involuntary muscle response in patients [22]. Alternatives includes random step levels or pseudo-random multi-level sequences.

4.2. Evaluation Method

In this study, the 1^{st} and 3^{rd} sets of input/output data are used to identify a model associated with predicted output $\hat{y}$, and the remaining sets are used for validating the model on a new input/output set. The fitness of cross-validation is expressed in terms of Best Fit value, defined as the percentage

$$\text{Best Fit} = 100\left(1 - \frac{\|y_{i+1} - \hat{y}_{s_i}\|}{\|y_{i+1} - \overline{y}_{i+1}\|}\right)\%, \tag{27}$$

where $\hat{y}_{s_i}$ denotes the simulated output obtained from the model identified on trial i, and y_{i+1} is the experimental output on validation trial $i+1$. The mean value of y is denoted by $\bar{y}$. To calculate the fitness of validation, the term y_{i+1} is exchanged with y_i in (27).

Parameters m_P, n_P and l_P are varied within a set of range. Then for each delay order m_P, the fitness values calculated from all data sets of each participant are averaged in order to examine the effects of any changes in n_P or l_P on the model accuracy.

4.3. Evaluation Results

The variation in the average fitness values calculated from two experimental data sets is shown for Participant P4 in Fig. 7 and Fig. 8 where n_P and l_P are each varied from 1 to 100 for several fitness values of m_P and the colorbar indicates the percent fitness values. Fig. 7 and Fig. 8 show averaged fitness values calculated from validation and cross-validation tests, respectively. As can be seen from Fig. 8, m_P should be chosen equal to 1 because increasing m_P causes a decrease in the Best Fit value.

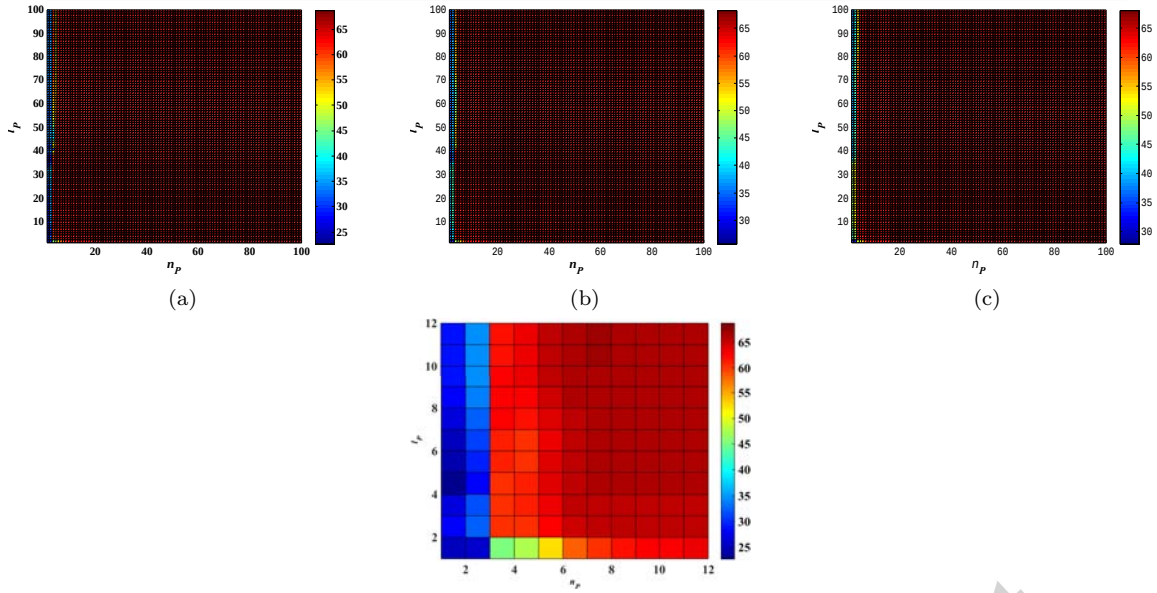

(a) (b) (c)

(d)

Fig. 8: Variation in averaged Best Fit values of ARX models identified using 1^{st} and 2^{nd} data set of Participant P4 when l_P and n_P are varied from 1 to 100 in (a) (b) and (c), where $m_P = 1$, $m_P = 2$ and $m_P = 3$, respectively and from 1 to 12 in (d) where $m_P = 1$. These values are obtained from cross-validation tests.

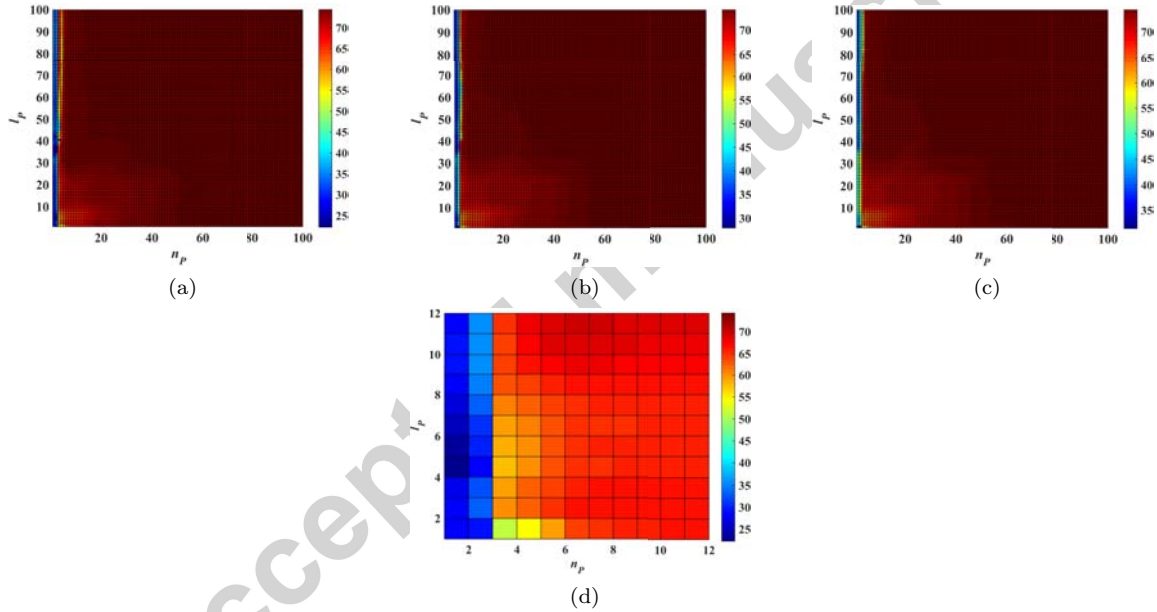

(a) (b) (c)

(d)

Fig. 7: Variation in averaged Best Fit values of ARX models identified using 1^{st} and 2^{nd} data set of Participant P4 when l_P and n_P are varied from 1 to 100 in (a) (b) and (c), where $m_P = 1$, $m_P = 2$ and $m_P = 3$, respectively and from 1 to 12 in (d) where $m_P = 1$. These values are obtained from validation tests.

From Fig. 7 and Fig. 8, it is evident that increasing the values of l_P and n_P results in increasing the Best Fit values of validation and cross-validation. Similar results were observed with the other participants. For example, the average fitness values of validation tests are found as 82.55% for Participant P1, 74.67% for Participant P2, 72.09% for Participant P3 and 78.73% for Participant P4 when both n_P and l_P are set to 250. The averaged fitness values of cross-validation tests for the same values of l_P and n_P are calculated as 71.22% for Participant P1, 68.31% for Participant P2, 60.50% for Participant P3 and 70.39% for Participant P4. These results evidently show that higher values give rise to higher accuracy. However limitations in computational resources may necessitate a lower order plant model to be identified. Thus the effect of selecting lower values of l_P and n_P is next examined.

The computations are repeated with n_P and l_P kept within a narrow range between 4 and 12. Table 1 to Table 4 show the Best Fit values in terms of average fitness calculated using the two experimental data sets corresponding to each participant. Table 5 shows the overall average Best Fit values calculated using the values from Table 1 to Table 4.

Table 1: Averaged Best Fit values (%) of n_P and l_P for Participant P1 when $m_P = 1$

l_P / n_P		4	5	6	7	8	9	10	11	12
4	CV	57.75	57.48	57.64	57.67	58.00	59.00	60.21	61.21	61.87
	V	61.44	61.48	61.95	62.06	62.30	63.18	64.38	65.42	66.11
5	CV	60.15	60.43	60.30	60.31	60.39	60.97	61.93	62.83	63.48
	V	63.78	64.69	64.55	64.68	64.74	65.21	66.11	67.01	67.65
6	CV	63.57	63.47	63.41	63.81	63.86	64.04	64.52	65.12	65.66
	V	67.14	67.64	67.93	68.19	68.23	68.37	68.80	69.36	69.84
7	CV	66.55	66.17	65.93	65.89	66.62	66.76	66.91	67.19	67.52
	V	70.10	70.26	70.33	70.35	70.96	71.09	71.25	71.49	71.74
8	CV	68.53	68.01	67.68	67.62	67.69	68.41	68.54	68.64	68.79
	V	72.11	72.05	71.97	71.96	71.98	72.66	72.85	72.96	73.05
9	CV	69.71	69.15	68.79	68.74	68.85	68.97	69.52	69.60	69.65
	V	73.36	73.19	73.03	72.99	73.05	73.13	73.74	73.88	73.92
10	CV	70.43	69.87	69.51	69.47	69.62	69.77	69.87	70.21	70.24
	V	74.15	73.95	73.74	73.70	73.78	73.91	74.01	74.43	74.50
11	CV	70.94	70.41	70.05	70.03	70.19	70.37	70.48	70.52	70.70
	V	74.73	74.55	74.33	74.28	74.38	74.54	74.67	74.71	74.96
12	CV	71.33	70.84	70.48	70.45	70.62	70.81	70.93	70.97	70.98
	V	75.14	75.02	74.82	74.77	74.87	75.04	75.19	75.24	75.24

V: Validation, CV: Cross-Validation

Table 2: Averaged Best Fit values (%) of n_P and l_P for Participant P2 when $m_P = 1$

l_P / n_P		4	5	6	7	8	9	10	11	12
4	CV	57.15	57.42	57.56	57.92	58.03	57.63	56.83	56.12	55.70
	V	62.42	61.72	60.95	61.16	61.51	61.49	61.09	60.80	60.87
5	CV	57.99	57.90	57.98	58.41	58.59	58.31	57.73	57.24	56.91
	V	62.78	61.98	61.30	61.74	62.24	62.38	62.20	62.06	62.11
6	CV	58.20	58.12	58.04	58.46	58.60	58.31	57.75	57.28	56.98
	V	62.94	62.12	61.33	61.77	62.26	62.41	62.27	62.17	62.21
7	CV	58.51	58.56	58.58	58.75	58.82	58.43	57.81	57.31	56.97
	V	63.27	62.59	61.93	62.05	62.47	62.50	62.28	62.14	62.15
8	CV	58.54	58.75	58.91	59.09	58.98	58.53	57.90	57.41	57.05
	V	63.37	62.85	62.40	62.59	62.72	62.65	62.36	62.18	62.15
9	CV	58.29	58.60	58.86	59.04	58.88	58.42	57.83	57.38	57.05
	V	63.25	62.83	62.51	62.74	62.85	62.67	62.36	62.17	62.12
10	CV	58.00	58.32	58.62	58.79	58.62	58.14	57.59	57.18	56.89
	V	63.12	62.73	62.46	62.69	62.79	62.58	62.25	62.05	62.00
11	CV	57.88	58.13	58.42	58.59	58.41	57.90	57.32	56.93	56.67
	V	63.11	62.69	62.40	62.64	62.72	62.48	62.11	61.89	61.85
12	CV	58.09	58.24	58.49	58.66	58.48	57.94	57.31	56.88	56.63
	V	63.29	62.81	62.50	62.75	62.83	62.56	62.16	61.91	61.86

V: Validation, CV: Cross-Validation

Table 3: Averaged Best Fit values (%) of n_P and l_P for Participant P3 when $m_P = 1$

l_P / n_P		4	5	6	7	8	9	10	11	12
4	CV	54.98	56.38	57.50	57.71	57.80	58.25	58.68	58.82	58.76
	V	55.83	56.67	57.67	57.91	58.11	58.60	59.03	59.19	59.22
5	CV	55.45	57.21	57.87	58.13	58.17	58.51	58.90	59.02	58.95
	V	56.53	57.90	58.26	58.55	58.68	59.03	59.38	59.52	59.52
6	CV	56.78	58.21	59.34	59.25	59.27	59.45	59.69	59.77	59.68
	V	58.96	59.84	60.60	60.59	60.67	60.83	61.02	61.09	61.09
7	CV	58.04	59.19	60.05	60.13	60.24	60.36	60.48	60.50	60.40
	V	61.67	62.11	62.49	62.54	62.81	62.91	62.96	62.95	62.93
8	CV	58.78	59.78	60.46	60.48	60.49	60.75	60.83	60.84	60.77
	V	63.80	64.00	64.12	64.07	64.12	64.53	64.55	64.53	64.50
9	CV	58.99	59.96	60.55	60.54	60.55	60.68	60.74	60.74	60.71
	V	65.11	65.24	65.24	65.14	65.20	65.33	65.58	65.57	65.58
10	CV	58.86	59.88	60.47	60.45	60.45	60.56	60.59	60.44	60.41
	V	65.78	65.94	65.92	65.81	65.88	66.05	66.09	66.21	66.23
11	CV	58.65	59.70	60.32	60.30	60.30	60.40	60.40	60.30	60.06
	V	66.05	66.30	66.31	66.20	66.28	66.47	66.54	66.54	66.63
12	CV	58.52	59.55	60.19	60.18	60.18	60.27	60.24	60.10	59.94
	V	66.14	66.46	66.52	66.41	66.49	66.69	66.78	66.78	66.79

V: Validation, CV: Cross-Validation

Table 4: Averaged Best Fit values (%) of n_P and l_P for Participant P4 when $m_P = 1$

l_P / n_P		4	5	6	7	8	9	10	11	12
4	CV	60.85	63.81	65.76	66.20	66.20	66.06	65.99	66.02	66.14
	V	60.44	63.21	64.94	65.37	65.49	65.50	65.51	65.62	65.89
5	CV	60.74	63.91	65.70	66.16	66.18	66.07	65.99	66.03	66.13
	V	60.48	63.64	64.96	65.45	65.63	65.68	65.70	65.79	66.04
6	CV	60.79	63.61	65.54	65.97	66.02	65.95	65.90	65.94	66.04
	V	60.69	63.20	64.81	65.14	65.38	65.49	65.54	65.64	65.85
7	CV	61.68	64.18	65.69	66.14	66.09	66.02	65.98	66.03	66.13
	V	62.15	64.24	65.21	65.60	65.64	65.75	65.83	65.93	66.10
8	CV	62.81	64.76	66.05	66.35	66.30	66.18	66.14	66.19	66.30
	V	64.57	65.86	66.50	66.59	66.64	66.62	66.69	66.79	66.95
9	CV	63.43	65.25	66.29	66.56	66.48	66.33	66.28	66.33	66.45
	V	66.54	67.62	67.85	67.83	67.74	67.68	67.70	67.79	67.93
10	CV	63.44	65.38	66.41	66.62	66.55	66.40	66.32	66.36	66.47
	V	67.49	68.76	68.94	68.79	68.66	68.55	68.51	68.63	68.78
11	CV	63.17	65.20	66.33	66.57	66.51	66.37	66.29	66.29	66.36
	V	67.92	69.40	69.70	69.57	69.40	69.27	69.24	69.28	69.52
12	CV	62.92	64.98	66.18	66.48	66.44	66.33	66.25	66.23	66.27
	V	68.06	69.74	70.20	70.14	69.98	69.84	69.81	69.87	70.02

V: Validation, CV: Cross-Validation

Table 5: Averaged Best Fit values (%) of n_P and l_P for all participants when $m_P = 1$

l_P \ n_P		4	5	6	7	8	9	10	11	12
4	CV	57.68	58.77	59.62	59.87	60.01	60.24	60.43	60.54	60.62
	V	60.03	60.77	61.38	61.63	61.85	62.19	62.50	62.76	63.03
5	CV	58.58	59.86	60.46	60.75	60.83	60.96	61.14	61.28	61.37
	V	60.89	62.05	62.26	62.61	62.82	63.07	63.35	63.60	63.83
6	CV	59.83	60.85	61.58	61.87	61.94	61.94	61.97	62.03	62.09
	V	62.43	63.20	63.67	63.92	64.13	64.27	64.41	64.57	64.75
7	CV	61.20	62.03	62.56	62.73	62.94	62.89	62.80	62.76	62.76
	V	64.29	64.80	64.99	65.13	65.47	65.56	65.58	65.63	65.73
8	CV	62.16	62.83	63.28	63.39	63.37	63.47	63.35	63.27	63.23
	V	65.96	66.19	66.25	66.30	66.36	66.62	66.61	66.61	66.66
9	CV	62.60	63.24	63.62	63.72	63.69	63.60	63.59	63.51	63.47
	V	67.06	67.22	67.16	67.18	67.21	67.20	67.35	67.35	67.39
10	CV	62.68	63.36	63.75	63.83	63.81	63.72	63.59	63.55	63.50
	V	67.63	67.84	67.76	67.75	67.78	67.77	67.72	67.83	67.88
11	CV	62.66	63.36	63.78	63.87	63.85	63.76	63.62	63.51	63.45
	V	67.96	68.23	68.19	68.17	68.19	68.19	68.14	68.10	68.24
12	CV	62.71	63.40	63.84	63.95	63.93	63.84	63.68	63.55	63.46
	V	68.16	68.51	68.51	68.52	68.54	68.54	68.48	68.45	68.48

V: Validation, CV: Cross-Validation

Validation and cross-validation Best Fit values in all tables are higher than 50% confirming that a sufficiently accurate lower order model was obtained for each participant. The highest fitness values, those greater than 70%, were obtained with Participant P1. However, the changes in Best Fit values of each participant are not significant when n_P and l_P are varied from 4 to 12. This is deduced from the mean and standard deviation of the Best Fit values in Table 1 to Table 4 which are 66.61 (4.12), 57.95 (0.73), 59.51 (1.26) and 65.57 (1.39) for cross-validation tests and 70.79 (4.12), 62.29 (0.55), 63.14 (3.23) and 66.76 (2.26) for validation tests, respectively. There are slight differences between the values in these tables.

Examination of the average Best Fit values in Table 5 enables suitable parameters to be selected that can subsequently be prescribed in future identification tests. Since these parameters provide confirmed accuracy, the procedure can be employed in clinical trials without the need to undertake cross-validation tests. When the Best Fit values in Table 5 are compared, the most suitable n_P and l_P values are found to be 7 and 12, respectively. With this choice, there is only a 1.08%, 14.13%, 0.53% and 5.55% degradation in accuracy of cross-validation for Participant P1, Participant P2, Participant P3 and Participant P4 with respect to the highest values of accuracy calculated when $l_P = m_P = 250$. Hence it can asserted that the use of lower values of n_P and l_P does not give rise to significant decrease in accuracy.

To confirm that the identified models provide a consistent representation of underlying dynamics, the frequency responses of some chosen models of two participants are plotted in Fig. 9 and Fig. 10. In these figures, it can clearly be seen that all frequency responses within the frequency range of input signal are similar. In Fig. 11, the comparison between the measured outputs used for validation and cross validation tests and the simulated output obtained from the model identified with $l_P = 12$, $n_P = 7$ and $m_P = 1$ is shown for Participant P1. Using an appropriate initial vector θ, Algorithm 1 achieved convergence typically within 75 iterations, with a computation time of less than 1 minute. The convergence is illustrated by Fig. 12.

5. Conclusion

A nonlinear model structure has been proposed to model wrist joint dynamics for the purpose of tremor suppression. The model captures critical nonlinear recruitment characteristics to overcome the accuracy limitations of previous approaches, while simultaneously embedding muscle co-activation to reduce deadzone and produce a SISO model. The overall structure can be linearised in a transparent manner in order to extend the range of admissible control schemes for subsequent tremor suppression. The proposed identification procedure is of short duration, can be automated, and is appropriate for use

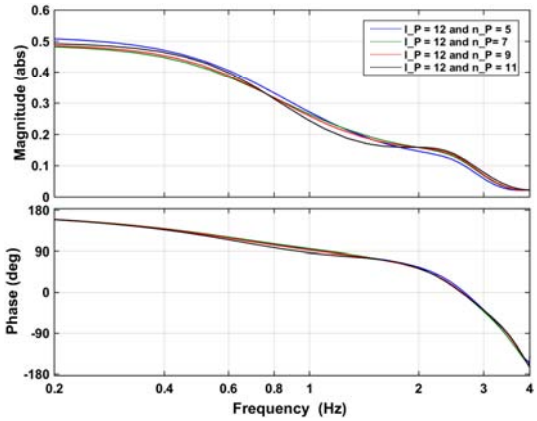

Fig. 9: Bode plots of models identified using 2^{nd} data set of Participant P2 with different values of n_P when $l_P = 12$ and $m_P = 1$.

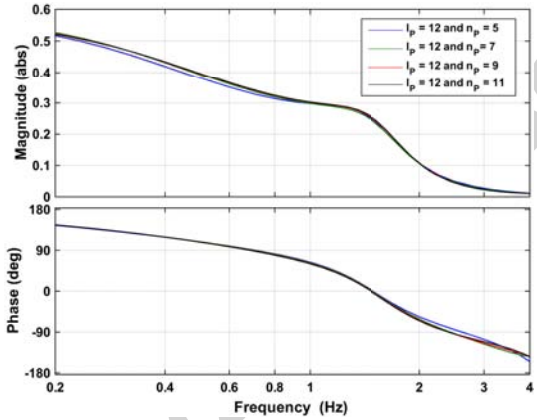

Fig. 10: Bode plots of models identified using 1^{st} data set of Participant P1 with different values of n_P when $l_P = 12$ and $m_P = 1$.

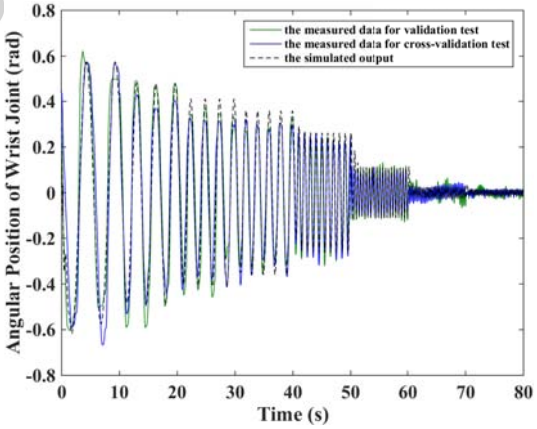

Fig. 11: The comparisons of validation data, cross-validation data and time response of the model identified using 1^{st} data set of Participant P1 with the values of when $l_P = 12$, $n_P = 7$ and $m_P = 1$.

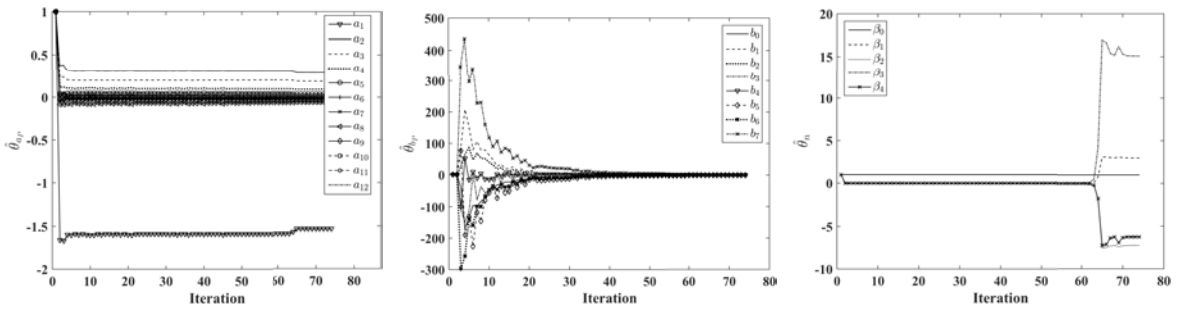

(a) (b) (c)

Fig. 12: An example of convergence property for Algorithm 1 are presented: (a) the change of $\hat{\theta}_{a_P}$ at each iteration (b) the change of $\hat{\theta}_{b_P}$ at each iteration (c) the change of $\hat{\theta}_n$ at each iteration. Convergence is achieved after 74 iterations.

by both patients and clinicians, thereby addressing major shortcomings encountered in previous studies. Note that the SISO system is obtained based on the assumption that the FCR and ECR muscles have similar linear activation dynamics. If this is not the case, then the system model becomes a multi-input single-output (MISO) system including two different Hammerstein structures arranged in parallel and then connected in cascade with the joint dynamics. Established identification methods for MISO Hammerstein systems [6, 21] can be adopted to solve such an identification problem. This forms part of our future research and will be reported separately.

Experimental results have confirmed satisfactory modelling accuracy, with cross-validation tests giving rise to a fitting accuracy of over 60% in all participants tested. Moreover, they confirm that a prescribed parameter set can be fixed for all participants with only minor degradation in accuracy, further reducing the identification time required.

Future work will involve applying the proposed identification approach clinically, requiring inclusion of tremor component, followed by model-based control design and implementation. This is significantly simplified since the proposed model structure may be linearised in a transparent manner enabling a wide range of designs to be employed. Future work will also focus on implementing the proposed algorithm in real-time to update the model parameters during closed-loop operation. This requires reformulating the proposed algorithm in a recursive form, following the approach of [23].

6. References

[1] E.-W. Bai, Z. Cai, S. Dudley-Javoroskv, and R. K. Shields. Identification of a modified Wiener-Hammerstein system and its application in electrically stimulated paralyzed skeletal muscle modeling. *Automatica*, 45:736–743, 2009.

[2] A. P. L. Bo, C. Azevedo-Coste, P. Poignet, C. Geny, and C. Fattal. On the use of FES to attenuate tremor by modulating joint impedance. In *50th IEEE Conference on Decision and Control and European Control Conference*, pages 6498–6503, 2011.

[3] A. P. L. Bo and P. Poignet. Tremor attenuation using FES-based joint stiffness control. In *2010 IEEE International Conference on Robotics and Automation (ICRA)*, pages 2928–2933, May 2010.

[4] J. Bobet, E. Gossen, and R. Stein. A comparison of models of force production during stimulated isometric ankle dorsiflexion in humans. *IEEE Transactions on Neural Systems and Rehabilitation Engineering*, 13(4):444–451, 2005.

[5] J. Bobet and R. Stein. A simple model of force generation by skeletal muscle during dynamic isometric contractions. *IEEE Transactions on Biomedical Engineering*, 45(8):1010–1016, 1998.

[6] M. Boutayeb, M. Darouach, and P. M. Frank. Modeling and identification for highly nonlinear processes. *Mathematics and Computers in Simulation*, 46:551–557, 1998.

[7] F. M. Colacino, E. Rustighi, and B. R. Mace. Subject-specific musculoskeletal parameters of wrist flexors and extensors estimated by an EMG-driven musculoskeletal model. *Medical Engineering & Physics*, 34(5):531–40, 2012.

[8] M. Curtin and M. M. Lowery. Musculoskeletal modelling of muscle activation and applied external forces for the correction of scoliosis. *Journal of Neuroengineering and Rehabilitation*, 11(1):52, 2014.

[9] J. Ding, A. S. Wexler, and S. A. Binder-Macleod. A mathematical model that predicts the force-frequency relationship of human skeletal muscle. *Muscle & Nerve*, 26(4):477–485, 2002.

[10] W. K. Durfee and K. E. Maclean. Methods for estimating isometric recruitment curves of electrically stimulated muscle. *IEEE Transactions on Biomedical Engineering*, 36(7):654–666, 1989.

[11] R. J. Elble. Tremor: clinical features, pathophysiology, and treatment. *Neurologic Clinics*, 3:177–185, 2009.

[12] P. Feys, W. Helsen, X. Liu, D. Mooren, H. Albrecht, B. Nuttin, and P. Ketelaer. Effects of peripheral cooling on intention tremor in multiple sclerosis. *Journal of Neurology, Neurosurgery and Psychiatry*, 76(3):373–379, 2005.

[13] C. T. Freeman, A.-M. Hughes, J. H. Burridge, P. H. Chappell, P. L. Lewin, and E. Rogers. A model of the upper extremity using FES for stroke rehabilitation. *Journal of Biomechanical Engineering*, 131(3):031011–12pp, 2009.

[14] B. Freriks, H. J. Hermens, C. Disselhorst-Klug, and G. Rau. *SENIAM 8: European Recommendations for Surface ElectroMyoGraphy*, Chapter 2: The Recommendations for Sensors and Sensor Placement Procedures for Surface ElectroMyoGraphy. Roessingh Research and Development, 1999.

[15] L. A. Frey Law and R. K. Shields. Mathematical models of human paralyzed muscle after long-term training. *Journal of Biomechanics*, 40(12):2587–2595, 2007.

[16] J. A. Gallego, J. Ibanez, J. Dideriksen, J. Serrano, M. del Castillo, D. Farina, and E. Rocon. A multimodal human-robot interface to drive a neuroprosthesis for tremor management. *IEEE Transactions on Systems, Man, and Cybernetics, Part C: Applications and Reviews,*, 42(6):1159–1168, 2012.

[17] J. A. Gallego, E. Rocon, J. M. Belda-Lois, and J. L. Pons. A neuroprosthesis for tremor management through the control of muscle co-contraction. *Journal of NeuroEngineering and Rehabilitation*, 10(1), 2013.

[18] A. Hassan, J. E. Ahlskog, M. Rodriguez, and J. Y. Matsumoto. Surgical therapy for multiple sclerosis tremor: a 12-year follow-up study. *European Journal of Neurology*, 19(5):764–768, 2012.

[19] K. J. Hunt, M. Munih, N. d. Donaldson, and F. M. D. Barr. Investigation of the Hammerstein hypothesis in the modeling of electrically stimulated muscle. *IEEE Transactions on Biomedical Engineering*, 45(8):998–1009, 1998.

[20] J. M. Iaquinto and J. S. Wayne. Computational model of the lower leg and foot/ankle complex: application to arch stability. *Journal of Biomechanical Engineering*, 132(2):021009, 2010.

[21] M. Kortmann and H. Unbehauen. Identification method for nonlinear MISO systems. In *IFAC 10th Triennial World Congress*, pages 233–238, Munich, Germany, 1987.

[22] F. Le, I. Markovsky, C. T. Freeman, and E. Rogers. Identification of electrically stimulated muscle models of stroke patients. *Control Engineering Practice*, 18(4):396–407, 2010.

[23] F. Le, I. Markovsky, C. T. Freeman, and E. Rogers. Recursive identification of Hammerstein systems with application to electrically stimulated muscle. *Control Engineering Practice*, 20(4):386 – 396, 2012.

[24] L. Ljung. *Systen Identification Theory for the User*, Chapter 3: Simulation and Prediction, pages 66–69. Prentice-Hall, second edition, 1999.

[25] C. L. Lynch and M. R. Popovic. Functional electrical stimulation. *IEEE Control System Magazine*, 28(2):40–50, 2008.

[26] K. E. Lyons and R. Pahwa. Deep brain stimulation and tremor. *Neurotherapeutics*, 5(2):331 – 338, 2008.

[27] K. A. Mann, F. W. Werner, and A. K. Palmer. Frequency spectrum analysis of wrist motion for activities of daily living. *Journal of Orthopedic Research*, 7(5):304–306, 1989.

[28] M. Manto, E. Rocon, J. Pons, J. M. Belda, and S. Camut. Evaluation of a wearable orthosis and an associated algorithm for tremor suppression. *Physiological Measurement*, 28(4):415–425, 2007.

[29] M.-U. Manto. *The cerebellum and its disorders*, Chapter 7: Clinical signs of cerebellar disorders, pages 97–111. Cambridge University Press, 2001.

[30] V. Nekoukar and A. Erfanian. An adaptive fuzzy sliding-mode controller design for walking control with functional electrical stimulation: A computer simulation study. *International Journal of Control, Automation and Systems*, 9(6):1124–1135, 2011.

[31] R. O'Connor and M. U. Kini. Non-pharmacological and non-surgical interventions for tremor: a systematic review. *Parkinsonism Related Disorders*, 17(7):509–515, 2011.

[32] D. Popovic, R. B. Stein, M. N. Oguztoreli, M. Lebiedowska, and S. Jonic. Optimal control of walking with functional electrical stimulation: A computer simulation study. *IEEE Transactions on Rehabilitation Engineering*, 7(1):69–79, 1999.

[33] A. Prochazka, J. Elek, and M. Javidan. Attenuation of pathological tremors by functional electrical stimulation. I: Method. *Annals of Biomedical Engineering*, 20(2):205–224, 1992.

[34] A. Prochazka, J. Elek, and M. Javidan. Attenuation of pathological tremors by functional electrical stimulation. II: Clinical evaluation. *Annals of Biomedical Engineering*, 20(2):225–236, 1992.

[35] E. Rocon, A. F. Ruiz, F. Brunetti, J. L. Pons, J. M. Belda-Lois, and J. J. Sanchez-Lacuesta. On the use of an active wearable exoskeleton for tremor suppression via biomechanical loading. In *Proceedings of the 2006 IEEE International Conference on Robotics and Automation*, pages 3140–3145, 2006.

[36] P. R. Schuurman, D. A. Bosch, P. M. M. Bossuyt, G. J. Bonsel, E. J. W. Van Someren, R. M. A. De Bie, M. P. Merkus, and J. D. Speelman. A comparison of continuos thalamic stimulation and thalamotomy for suppression of severe tremor. *The New England Journal of Medicine*, 342(7):461–468, 2000.

[37] S. Takehara, M. Murakami, and K. Hase. Biomechanical evaluation of an electric power-assisted bicycle by a musculoskeletal model. *Journal of System Design and Dynamics*, 6(3):343–350, 2012.

[38] R. R. Tasker. Deep brain stimulation is preferable to thalamotomy for tremor suppression. *Surgical Neurology*, 49(2):143–153, 1998.

[39] A. K. Thompson, B. Doran, and R. B. Stein. Short-term effects of functional electrical stimulation on spinal excitatory and inhibitory reflexes in ankle extensor and flexor muscles. *Experimental Brain Research*, 170(2):216–226, 2006.

[40] C. V. Torres, E. Moro, A. L. Lopez-Rios, M. Hodaie, H. M., R. Chen, A. W. Laxton, W. D. Hutchison, J. O. Dostrovsky, and A. M. Lozano. Deep brain stimulation of the ventral intermediate nucleus of the thalamus for tremor in patients with multiple sclerosis. *Neurosurgery*, 67(3):646–651, 2010.

[41] R. Turk, S. V. Notley, R. M. Pickering, D. M. Simpson, P. A. Wright, and J. H. Burridge. Reliability and sensitivity of a wrist rig to measure motor control and spasticity in post-stroke hemiplegia. *Neurorehabilitation and Neural Repair*, 22(6):684–696, 2008.

[42] R. J. L. M. Verstappen, C. T. Freeman, E. Rogers, T. Sampson, and J. H. Burridge. Robust higher order repetitive control applied to human tremor suppression. In *IEEE Multi-Conference on Systems and Control*, pages 1214–1219, 2012.

[43] WHO and MSIF. Multiple sclerosis resources in the world 2008. Technical report, World Health Organization and Multiple Sclerosis International Federation, 2008.

[44] L. Yap, A. Kouyialis, and T. R. K. Varma. Stereotactic neurosurgery for disabling tremor in multiple sclerosis: thalamotomy or deep brain stimulation?. *British Journal of Neurosurgery*, 21(4):349–354, 2007.

[45] D. Zhang and W. T. Ang. Tremor suppression of elbow joint via functional electrical stimulation: a simulation study. In *Proceeding of the 2006 IEEE International Conference on Automation Science and Engineering*, pages 182–187, 2006.

[46] D. Zhang and W. T. Ang. *Mechanisms and Emerging Therapies in Tremor Disorders*, Chapter 5: Musculoskeletal Models of Tremor, pages 79–107. Springer Science & Business Media, 2012.

[47] D. Zhang, P. Poignet, F. Widjaja, and W. T. Ang. Neural oscillator based control for pathological tremor suppression via functional electrical stimulation. *Control Engineering Practice*, 19(1):74–88, 2011.